High-performance Computing for the Geodynamo

Alexandre Fournier (IPGP) fournier@ipgp.fr
Thomas Gastine (IPGP/CNRS)
Nathanaël Schaeffer (ISTerre/CNRS)

Institut de Physique du Globe, Paris, France

March 11th, 2019

SIAM Conference on Mathematical & Computational Issues in the Geosciences

Outline

The geodynamo

Solution method

State-of-the-art simulations

Reversals

The Earth's interior and the geomagnetic field

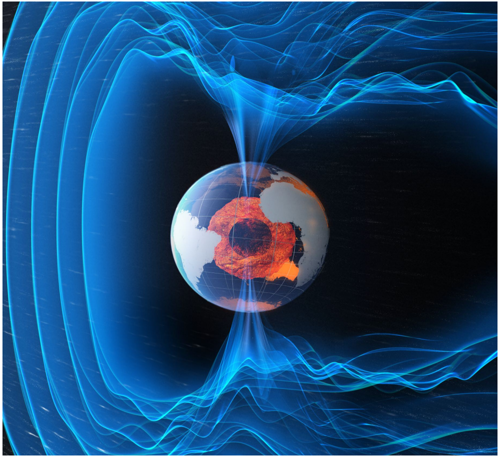

© European Space Agency (www.esa.int/swarm)

The Earth's interior and the geomagnetic field

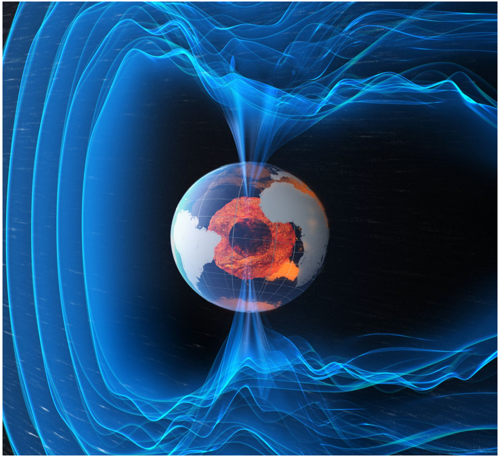

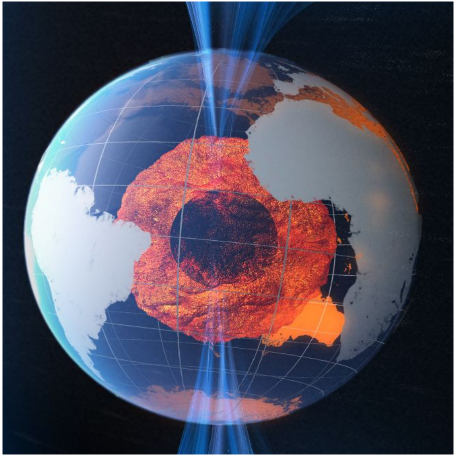

The Earth's interior and the geomagnetic field

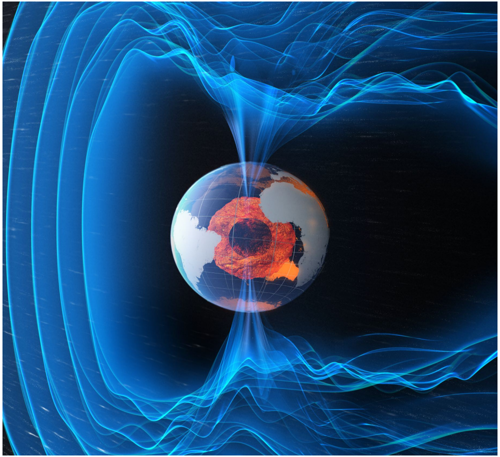

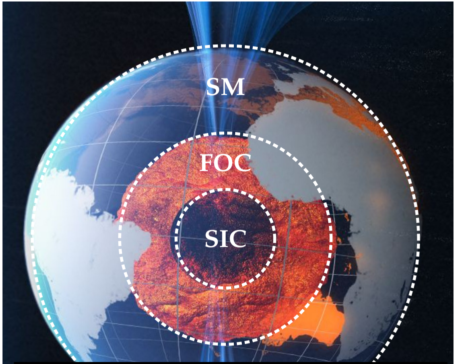

SM: Solid Mantle (rocks),	0–2890 km depth
FOC: Fluid Outer Core (liquid Fe),	2890–5150 km depth
SIC: Solid Inner Core (solid Fe),	5150–6370 km depth

The geomagnetic field: a sparse record (in space and time)

A short-sighted view

- dipole-dominated
- small scales of dynamo field concealed by the small scales of the crustal field
- even if perfect sampling: $\ell \lesssim 13$ (lateral resolution of $\sim$ 1500 km at the core surface)

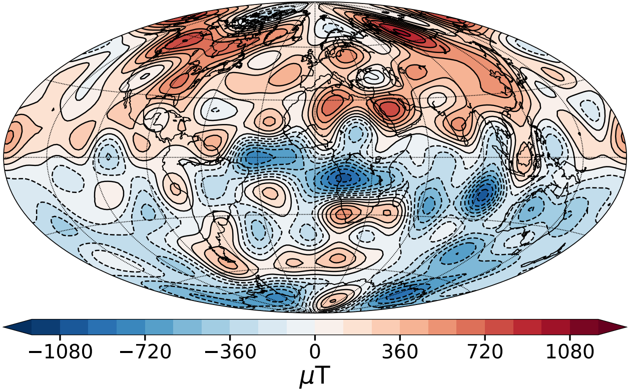

The geomagnetic field: a sparse record (in space and time)

A short-sighted view

- dipole-dominated
- small scales of dynamo field concealed by the small scales of the crustal field
- even if perfect sampling: $\ell \lesssim 13$ (lateral resolution of ~ 1500 km at the core surface)

Time variations : constraints provided by geomagnetism (observatory and satellite data)

- Smooth decadal variations punctuated by rapid (interannual) impulses (geomagnetic jerks)

Constraints provided by paleomagnetism

- The strength of the field varies on secular, millennial and geological time scales
- The further in the past we look, the cruder our description of the field (axial dipole)
- The field reverses its polarity every once in a while (≈ 4 Myr^{-1} over the past 25 Myr)
- Last one 780 ka, poorly constrained transitional field

First-principle simulations can complement observations

Numerical models of the geodynamo – the problem at hand

The Earth's dynamo is powered by convection. In its simplest Boussinesq form, using the codensity formalism (Braginsky and Roberts, 1995), the problem reads

$$
\begin{aligned}
\boldsymbol{\nabla} \cdot \boldsymbol{u} &= 0, \\
\rho_0 \partial_t \boldsymbol{u} &= \boldsymbol{F}_p + \boldsymbol{F}_C + \boldsymbol{F}_i + \boldsymbol{F}_L + \boldsymbol{F}_v + \boldsymbol{F}_b, \\
\partial_t C &= -\boldsymbol{u} \cdot \boldsymbol{\nabla} C + \kappa \nabla^2 C, \\
\partial_t \boldsymbol{B} &= \boldsymbol{\nabla} \times (\boldsymbol{u} \times \boldsymbol{B}) + \lambda \nabla^2 \boldsymbol{B}, \\
\boldsymbol{\nabla} \cdot \boldsymbol{B} &= 0.
\end{aligned}
$$

Forces

- $\boldsymbol{F}_p$ pressure
- $\boldsymbol{F}_C$ Coriolis (lin. in $\boldsymbol{u}$)
- $\boldsymbol{F}_i$ inertia (quad. in $\boldsymbol{u}$)
- $\boldsymbol{F}_L$ Lorentz (quad. in $\boldsymbol{B}$)
- $\boldsymbol{F}_v$ viscous (lin. in $\boldsymbol{u}$)
- $\boldsymbol{F}_b$ buoyancy (lin. in C)

Numerical models of the geodynamo – the problem at hand

The Earth's dynamo is powered by convection. In its simplest form – co-density formalism (Braginsky and Roberts, 1995), Boussinesq approximation

$$
\begin{aligned}
\nabla \cdot \boldsymbol{u} &= 0, \\
\rho_0 \partial_t \boldsymbol{u} &= \boldsymbol{F}_p + \boldsymbol{F}_C + \boldsymbol{F}_i + \boldsymbol{F}_L + \boldsymbol{F}_v + \boldsymbol{F}_b, \\
\partial_t C &= -\boldsymbol{u} \cdot \nabla C + \kappa \nabla^2 C, \\
\partial_t \boldsymbol{B} &= \nabla \times (\boldsymbol{u} \times \boldsymbol{B}) + \lambda \nabla^2 \boldsymbol{B}, \\
\nabla \cdot \boldsymbol{B} &= 0.
\end{aligned}
$$

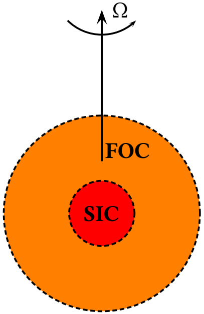

FOC: Fluid Outer Core	2890–5150 km depth
SIC: Solid Inner Core	5150–6370 km depth

+ initial and boundary conditions: no-slip at CMB and ICB, insulating BC at CMB, conducting inner core, Neumann or Dirichlet conditions for C.

Solution method - spatial discretization

Pioneered by Glatzmaier (1984) for the solar dynamo, still adopted by most codes 35 years later (Matsui et al., 2016)

- Poloidal-toroidal decomposition of solenoidal fields

$$\boldsymbol{u}(\boldsymbol{r},t) = \boldsymbol{\nabla}\times\boldsymbol{\nabla}\times[\mathcal{P}^{\boldsymbol{u}}(\boldsymbol{r},t)\boldsymbol{r}]+\boldsymbol{\nabla}\times[\mathcal{T}^{\boldsymbol{u}}(\boldsymbol{r},t)\boldsymbol{r}]\,, \quad \boldsymbol{B}(\boldsymbol{r},t) = \boldsymbol{\nabla}\times\boldsymbol{\nabla}\times\left[\mathcal{P}^{\boldsymbol{B}}(\boldsymbol{r},t)\boldsymbol{r}\right]+\boldsymbol{\nabla}\times\left[\mathcal{T}^{\boldsymbol{B}}(\boldsymbol{r},t)\boldsymbol{r}\right]$$

- The horizontal dependency is handled by means of spherical harmonics, e. g.

$$\mathcal{P}^{\boldsymbol{u}}(\boldsymbol{r},t) \approx \sum_{\ell=0}^{\ell=\ell_{\max}} \sum_{m=-m_{\max}}^{m=m_{\max}} \mathcal{P}^{\boldsymbol{u}}_{\ell m}(r,t)\mathcal{Y}_{\ell}^{m}(\theta,\varphi)$$

- Radial dependency: finite-difference or Chebyshev polynomials

Solution method - temporal discretization

One ends up with the following generic equation to time step

$$\frac{\mathrm{d}\mathbf{x}}{\mathrm{d}t} = \boldsymbol{f}_{\text{L}}(\mathbf{x}) + \boldsymbol{f}_{\text{NL}}(\mathbf{x}),$$

in which $\mathbf{x}$ is the complex-valued state vector.

Implicit–Explicit (IMEX) scheme

- Implicit for $\boldsymbol{f}_{\text{L}}(\mathbf{x})$
- Explicit for $\boldsymbol{f}_{\text{NL}}(\mathbf{x})$ (computed in physical space – pseudo-spectral approach), one round-trip per evaluation of $\boldsymbol{f}_{\text{NL}}(\mathbf{x})$
- Most codes resort to second order IMEX (CNAB2, CNAB3) with adaptive time-stepping

What the ideal geodynamo simulation should achieve

- produce a geomagnetic secular variation similar to the observed one
- generate a dipole-dominated field whose morphology at the CMB is similar to that of the recent geomagnetic field up to degree 13
- operate in a strong-field regime (magnetic energy $\gg$ kinetic energy)
- produce a scale separation between $\boldsymbol{B}$ (large-scale) and $\boldsymbol{u}$ (small-scale)
- account for interannual geomagnetic impulses observed in the recent record
- produce irregular reversals of polarity over geological time scales

What the ideal geodynamo simulation should achieve

- produce a geomagnetic secular variation similar to the observed one
- generate a dipole-dominated field whose morphology at the CMB is similar to that of the recent geomagnetic field up to degree 13
- operate in a strong-field regime (magnetic energy $\gg$ kinetic energy)
- produce a scale separation between $\boldsymbol{B}$ (large-scale) and $\boldsymbol{u}$ (small-scale)
- account for interannual geomagnetic impulses observed in the recent record
- produce irregular reversals of polarity over geological time scales

This is contingent upon honoring the following separation of time scales

τ_Ω		τ_A		τ_adv		τ_λ
rotation	$\ll$	Alfvén	$\ll$	advection	$\ll$	mag diffusion
1 day		1 yr		100 yr		10^5 yr

over a simulation time spanning several million years ($\tau_\oplus$)

What current geodynamo simulations can achieve

- ✓ produce a geomagnetic secular variation similar to the observed one
- ✓ generate a dipole-dominated field whose morphology at the CMB is similar to that of the recent geomagnetic field up to degree 13

Christensen et al. (2010): The Earth-likeness is controlled by 2 ratios of 3 time scales

$$
\begin{aligned}
\mathrm{E}_\lambda &= \frac{\tau_\Omega}{\tau_\lambda} \\
\mathrm{Rm} &= \frac{\tau_\lambda}{\tau_{\mathrm{adv}}}
\end{aligned}
$$

$\mathrm{Rm} = O(1000)$ for Earth

What state-of-the-art geodynamo simulations can achieve

- ✓ operate in a strong-field regime (magnetic energy $\gg$ kinetic energy)
- ✓ produce a scale separation between $\boldsymbol{B}$ (large-scale) and $\boldsymbol{u}$ (small-scale)
- ✓ account for interannual geomagnetic impulses observed in the recent record

Schaeffer et al. (2017): current state-of-the-art for DNS

- $(Nr, \ell_{\max}, m_{\max}) = (1280, 1000, 893)$
- 10 million core hours
- $O(8000)$ cores
- Integration length: 8 τ_{adv} ($\sim$ 1000 yr)

The XSHELLS code

- FD in r, SH in (θ, φ)
- hybrid MPI/OpenMP parallelization
- Order 2 IMEX time scheme
- Uses the SHTns SH library (Schaeffer, 2013)
- open-source, available at https://bitbucket.org/nschaeff/xshells

What state-of-the-art geodynamo simulations can achieve

- ✓ operate in a strong-field regime (magnetic energy $\gg$ kinetic energy)
- ✓ produce a scale separation between $\boldsymbol{B}$ (large-scale) and $\boldsymbol{u}$ (small-scale)
- ✓ account for interannual geomagnetic impulses observed in the recent record

Schaeffer et al. (2017): current state-of-the-art for DNS

- $(Nr, \ell_{\max}, m_{\max}) = (1280, 1000, 893)$
- 10 million core hours
- $O(8000)$ cores
- Integration length: $8\ \tau_{\mathrm{adv}}$ ($\sim$ 1000 yr)

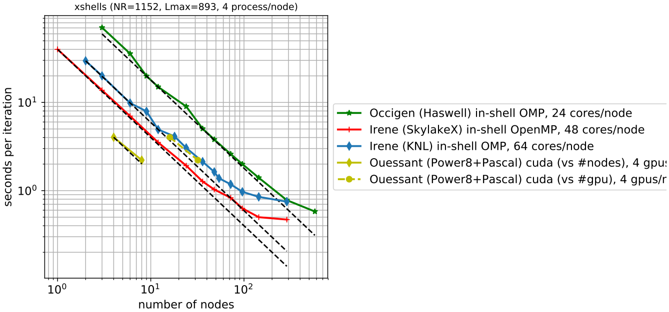

What state-of-the-art geodynamo simulations can achieve

- ✓ operate in a strong-field regime (magnetic energy $\gg$ kinetic energy)
- ✓ produce a scale separation between $\boldsymbol{B}$ (large-scale) and $\boldsymbol{u}$ (small-scale)
- ✓ account for interannual geomagnetic impulses observed in the recent record

Schaeffer et al. (2017): current state-of-the-art for DNS

- $(Nr, \ell_{\max}, m_{\max}) = (1280, 1000, 893)$
- 10 million core hours
- $O(8000)$ cores
- Integration length: $8\ \tau_{\mathrm{adv}}$ ($\sim$ 1000 yr)

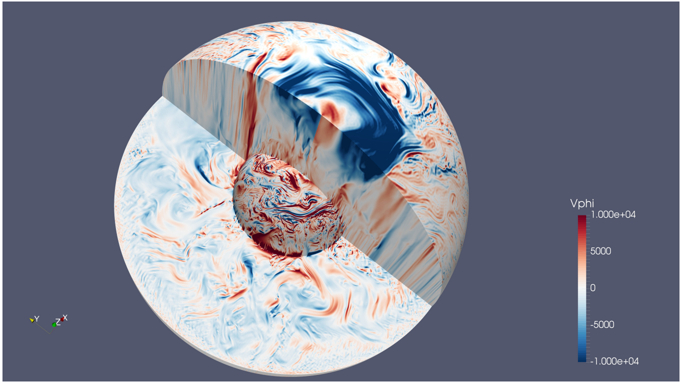

What state-of-the-art geodynamo simulations can achieve

✓ operate in a strong-field regime (magnetic energy $\gg$ kinetic energy)

✓ produce a scale separation between $\boldsymbol{B}$ (large-scale) and $\boldsymbol{u}$ (small-scale)

✓ account for interannual geomagnetic impulses observed in the recent record

Schaeffer et al. (2017): current state-of-the-art for DNS

- $(Nr, \ell_{\mathrm{max}}, m_{\mathrm{max}}) = (1280, 1000, 893)$
- 10 million core hours
- $O(8000)$ cores
- Integration length: $8\ \tau_{\mathrm{adv}}$ ($\sim$ 1000 yrs)

What state-of-the-art geodynamo simulations can achieve

- ✓ operate in a strong-field regime (magnetic energy $\gg$ kinetic energy)
- ✓ produce a scale separation between $\boldsymbol{B}$ (large-scale) and $\boldsymbol{u}$ (small-scale)

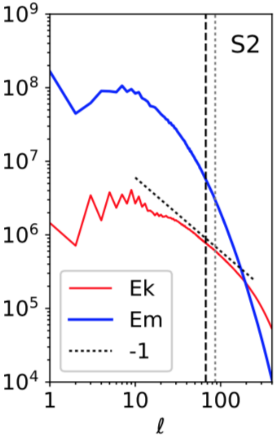

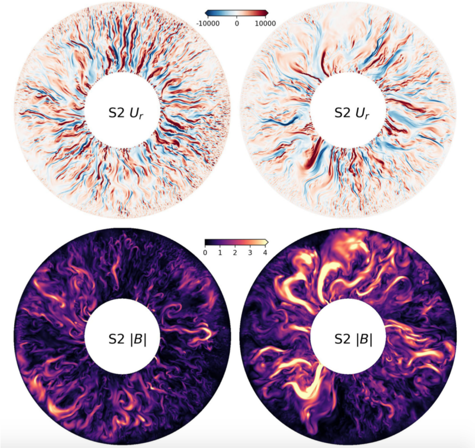

What state-of-the-art geodynamo simulations can achieve

✓ account for interannual geomagnetic impulses observed in the recent record: simulation exhibits waves of various kinds (torsional Alfvén waves, Magneto-Coriolis waves) thanks to reduced diffusivities

Torsional waves:

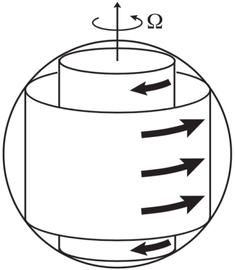

Figure 1. The geometry of the zonal flows in Earth's outer core which carry angular momentum. The depicted time varying zonal flows consist in either free Alfvén waves or forced accelerations.

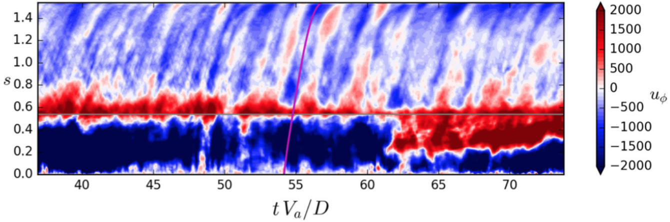

Schaeffer et al. (2017)

More and Dumberry (2017)

What the ideal geodynamo simulation should achieve

- ✓ produce a geomagnetic secular variation similar to the observed one
- ✓ generate a dipole-dominated field whose morphology at the CMB is similar to that of the recent geomagnetic field up to degree 13
- ✓ operate in a strong-field regime (magnetic energy $\gg$ kinetic energy)
- ✓ produce a scale separation between $\boldsymbol{B}$ (large-scale) and $\boldsymbol{u}$ (small-scale)
- ✓ account for interannual geomagnetic impulses observed in the recent record
- ✗ produce irregular reversals of polarity over geological time scales

$$\begin{array}{ccccccc} \tau_\Omega & & \tau_{\mathrm{A}} & & \tau_{\mathrm{adv}} & & \tau_\lambda \\ \text{rotation} & < & \text{Alfvén} & < & \text{advection} & < & \text{mag diffusion} \end{array}$$

over a simulation time spanning several ~~million years ($\tau_\oplus$)~~ τ_{adv}

Low-resolution reversal simulations

$(N_r, \ell_{\max}, m_{\max}) = (144, 79, 63)$ (3 orders of magnitude more viscous than state-of-the-art)

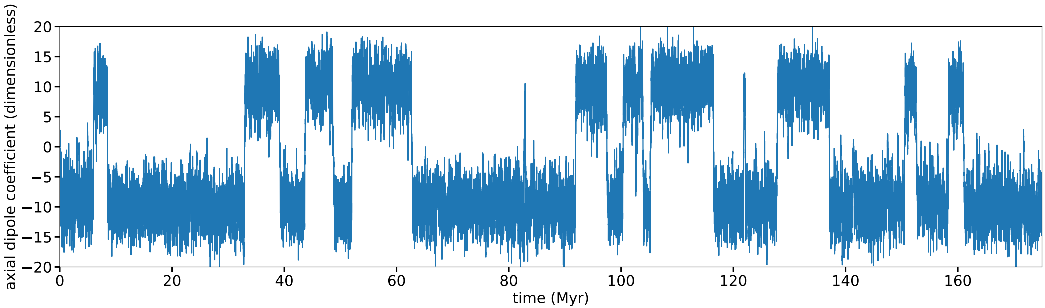

(600,000 core hours)

Low-resolution reversal simulations

$(N_r, \ell_{\max}, m_{\max}) = (144, 79, 63)$ (3 orders of magnitude more viscous than state-of-the-art)

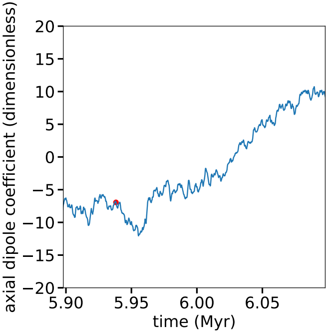

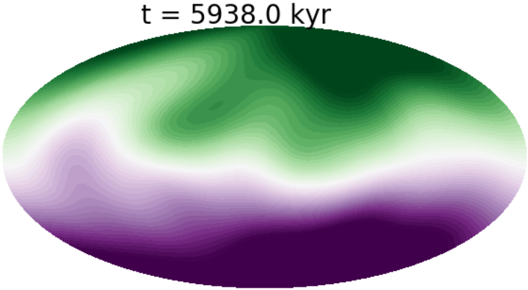

Low-resolution reversal simulations

$(N_r, \ell_{\text{max}}, m_{\text{max}}) = (144, 79, 63)$ (3 orders of magnitude more viscous than state-of-the-art)

Issues

- kinetic energy $\sim$ magnetic energy
- laminar, large-scale flow: no scale separation
- $\boldsymbol{F}_v$ and $\boldsymbol{F}_i$ too important in force balance
- Are those reversals relevant?

What to improve

Longer integration times with less viscous dynamos require a shorter time to solution.

Two possible options to explore

- Spatial discretization: sparse spectral representation in r
- Parallel in Time (PinT) approach

Sparse spectral representation

Goal: to benefit from spectral convergence in r while decreasing the memory imprint and improving the efficiency of a standard collocation approach

How: by generating (almost) banded matrices (Julien and Watson, 2009; Olver and Townsend, 2013; Marti et al., 2016).

Applied by Gastine (2019) to 2D spherical quasi-geostrophic convection

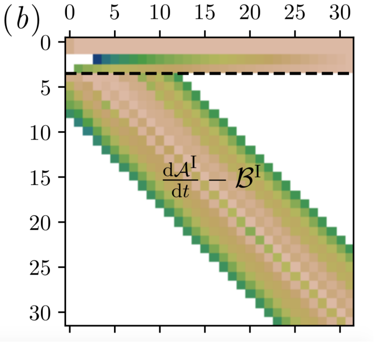

https://github.com/magic-sph/pizza

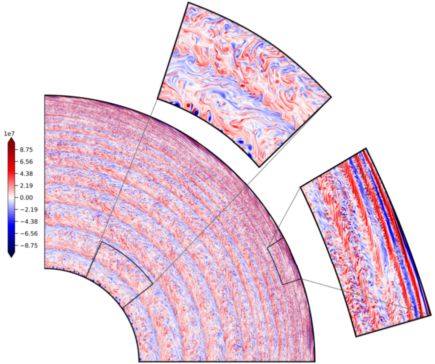

$(N_r, N_m) = (6145, 6144)$

PinT

Idea: enable extra domain decomposition when spatial parallelization is exhausted.

Possibilities: Parareal (Lions et al., 2001), PFASST (parallel full approximation scheme in space and time) (Emmett and Minion, 2012), ...

Clarke et al. (2019): application of Parareal to kinematic Cartesian dynamos

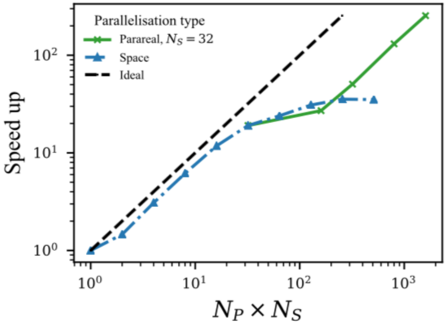

Galloway-Proctor flow, Rm $= 300$
N_s: # of procs. in space
N_p: # of procs. for parareal

Conclusion

The Geodynamo and HPC

- Current geodynamo simulations can run up to $O(10,000)$ cores (optimized SH transform library, MPI/OpenMP parallelization)
- Fair level of geophysical realism
- "turbulent state-of-the-art": time integration too short for reversals

Room for improvement: decrease time to solution

- sparse spectral methods
- PinT

Have to be assessed for the geodynamo problem

References I

Braginsky, S. I. and P. H. Roberts (1995). Equations governing convection in Earth's core and the geodynamo. *Geophysical & Astrophysical Fluid Dynamics 79*(1), 1–97.

Christensen, U. R., J. Aubert, and G. Hulot (2010). Conditions for Earth-like geodynamo models. *Earth and Planetary Science Letters 296*(3-4), 487–496.

Clarke, A. T., C. J. Davies, D. Ruprecht, and S. M. Tobias (2019). Parallel-in-time integration of kinematic dynamos. *arXiv preprint arXiv:1902.00387*.

Emmett, M. and M. Minion (2012). Toward an efficient parallel in time method for partial differential equations. *Communications in Applied Mathematics and Computational Science 7*(1), 105–132.

Fournier, A., L. Nerger, and J. Aubert (2013). An ensemble Kalman filter for the time-dependent analysis of the geomagnetic field. *Geochemistry, Geophysics, Geosystems 14*, 4035–4043. doi:10.1002/ggge.20252.

Gastine, T. (2019). pizza: an open-source pseudo-spectral code for spherical quasi-geostrophic convection. *Geophysical Journal International*.

Glatzmaier, G. A. (1984). Numerical simulations of stellar convective dynamos. I- The model and method. *Journal of Computational Physics 55*(3), 461–484.

Gubbins, D. and N. Roberts (1983). Use of the frozen flux approximation in the interpretation of archaeomagnetic and palaeomagnetic data. *Geophysical Journal of the Royal Astronomical Society 73*(3), 675–687.

Julien, K. and M. Watson (2009). Efficient multi-dimensional solution of pdes using chebyshev spectral methods. *Journal of Computational Physics 228*(5), 1480–1503.

References II

Lions, J. L., Y. Maday, and G. Turinici (2001). Résolution d'EDP par un schéma en temps pararéel. *Comptes Rendus de l'Académie des Sciences-Series I-Mathematics 332*(7), 661–668.

Marti, P., M. A. Calkins, and K. Julien (2016). A computationally efficient spectral method for modeling core dynamics. *Geochemistry, Geophysics, Geosystems 17*(8), 3031–3053.

Matsui, H., E. Heien, J. Aubert, J. M. Aurnou, M. Avery, B. Brown, B. A. Buffett, F. Busse, U. R. Christensen, C. J. Davies, N. Featherstone, T. Gastine, G. A. Glatzmaier, D. Gubbins, J.-L. Guermond, Y.-Y. Hayashi, R. Hollerbach, L. J. Hwang, A. Jackson, C. A. Jones, W. Jiang, L. H. Kellogg, W. Kuang, M. Landeau, P. Marti, P. Olson, A. Ribeiro, Y. Sasaki, N. Schaeffer, R. D. Simitev, A. Sheyko, L. Silva, S. Stanley, F. Takahashi, S.-i. Takehiro, J. Wicht, and A. P. Willis (2016). Performance benchmarks for a next generation numerical dynamo model. *Geochemistry, Geophysics, Geosystems 17*(5), 1586–1607.

More, C. and M. Dumberry (2017). Convectively driven decadal zonal accelerations in earth's fluid core. *Geophysical Journal International 213*(1), 434–446.

Olver, S. and A. Townsend (2013). A fast and well-conditioned spectral method. *SIAM Review 55*(3), 462–489.

Roberts, P. H. and S. Scott (1965). On analysis of the secular variation. 1. A hydromagnetic constraint: Theory. *Journal of Geomagnetism and Geoelectricity 17*(2), 137–151.

Schaeffer, N. (2013). Efficient spherical harmonic transforms aimed at pseudospectral numerical simulations. *Geochemistry, Geophysics, Geosystems 14*(3), 751–758.

Schaeffer, N., D. Jault, H.-C. Nataf, and A. Fournier (2017). Turbulent geodynamo simulations: a leap towards Earth's core. *Geophysical Journal International 211*(1), 1–29.

The internal field

Spherical harmonic analysis

$$
\begin{aligned}
\boldsymbol{B} &= -\boldsymbol{\nabla} V \text{ in a current-free region; with internal sources,} \\
V(r,\theta,\varphi,t) &= a \sum_{\ell,m} \left(\frac{a}{r}\right)^{\ell+1} \left[g_\ell^m(t)\cos m\varphi + h_\ell^m(t)\sin m\varphi\right] P_\ell^m(\cos\theta), \\
B_r(r,\theta,\varphi,t) &= \sum_{\ell,m} \left(\frac{a}{r}\right)^{\ell+2} \left[g_\ell^m(t)\cos m\varphi + h_\ell^m(t)\sin m\varphi\right] P_\ell^m(\cos\theta).
\end{aligned}
$$

Connection between surface observations and the field at the CMB

(CMB: Core-Mantle Boundary)

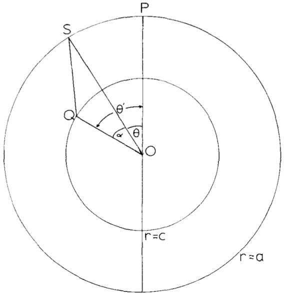

Figure 1. Geometry for the superposition integral (3). 0 is the origin of a system of spherical po coordinates with pole P. The site is at S(θ, ϕ) on the surface of the Earth. The Green's functi $N(Y, \theta, \phi; \theta', \phi')$, is the potential at S due to a singularity of unit strength in the radial field at poi (θ', ϕ') on the core–mantle boundary. N is symmetric about the axis OS and is a function only of the angular distance between Q and S. N is a maximum when Q is immediately beneath S, and decreas monotonically with increasing angular and distance α.

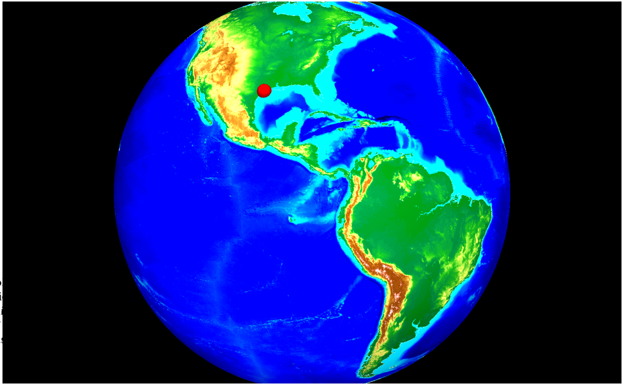

Gubbins and Roberts (1983)

Connection between surface observations and the field at the CMB

(CMB: Core-Mantle Boundary)

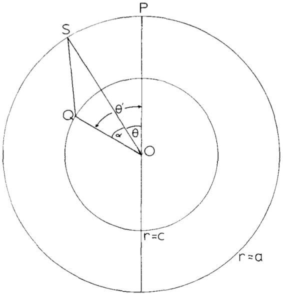

Figure 1. Geometry for the superposition integral (3). 0 is the origin of a system of spherical po coordinates with pole P. The site is at $S(\theta, \phi)$ on the surface of the Earth. The Green's functi $N(Y, \theta, \phi; \theta', \phi')$, is the potential at S due to a singularity of unit strength in the radial field at poi (θ', ϕ') on the core–mantle boundary. N is symmetric about the axis OS and is a function only of the angular distance between Q and S. N is a maximum when Q is immediately beneath S, and decreas monotonically with increasing angular and distance α.

Gubbins and Roberts (1983)

Connection between surface observations and the field at the CMB

(CMB: Core-Mantle Boundary)

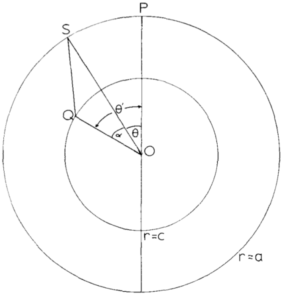

Figure 1. Geometry for the superposition integral (3). 0 is the origin of a system of spherical po coordinates with pole P. The site is at S(θ, ϕ) on the surface of the Earth. The Green's functi $N(Y, \theta, \phi; \theta', \phi')$, is the potential at S due to a singularity of unit strength in the radial field at poi (θ', ϕ') on the core–mantle boundary. N is symmetric about the axis OS and is a function only of the angular distance between Q and S. N is a maximum when Q is immediately beneath S, and decreas monotonically with increasing angular and distance α.

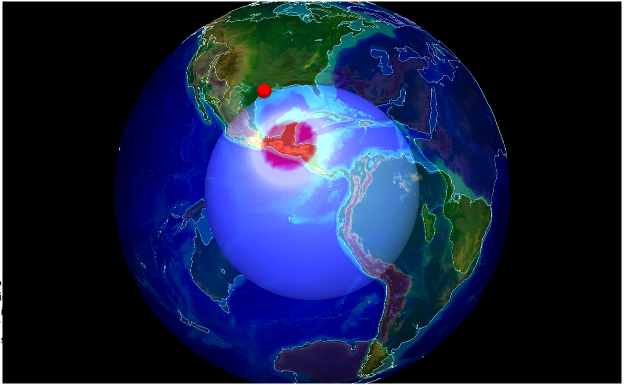

Gubbins and Roberts (1983)

Connection between surface observations and the field at the CMB

(CMB: Core-Mantle Boundary)

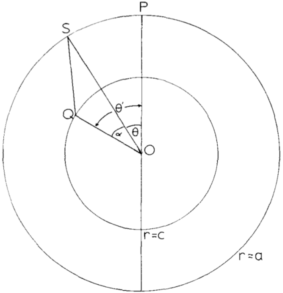

Figure 1. Geometry for the superposition integral (3). 0 is the origin of a system of spherical po coordinates with pole P. The site is at S(θ, ϕ) on the surface of the Earth. The Green's functi $N(Y, \theta, \phi; \theta', \phi')$, is the potential at S due to a singularity of unit strength in the radial field at poi (θ', ϕ') on the core–mantle boundary. N is symmetric about the axis OS and is a function only of the angular distance between Q and S. N is a maximum when Q is immediately beneath S, and decrea monotonically with increasing angular and distance α.

Gubbins and Roberts (1983)

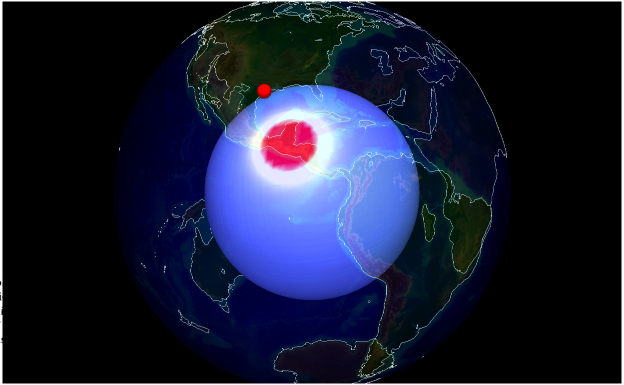

Connection between surface observations and the field at the CMB

(CMB: Core-Mantle Boundary)

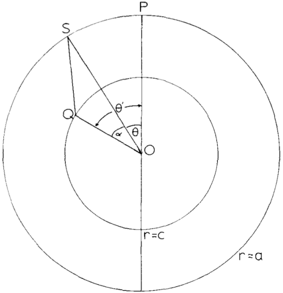

Figure 1. Geometry for the superposition integral (3). 0 is the origin of a system of spherical po coordinates with pole P. The site is at S(θ, ϕ) on the surface of the Earth. The Green's functi $N(Y, \theta, \phi; \theta', \phi')$, is the potential at S due to a singularity of unit strength in the radial field at poi (θ', ϕ') on the core–mantle boundary. N is symmetric about the axis OS and is a function only of the angular distance between Q and S. N is a maximum when Q is immediately beneath S, and decreas monotonically with increasing angular and distance α.

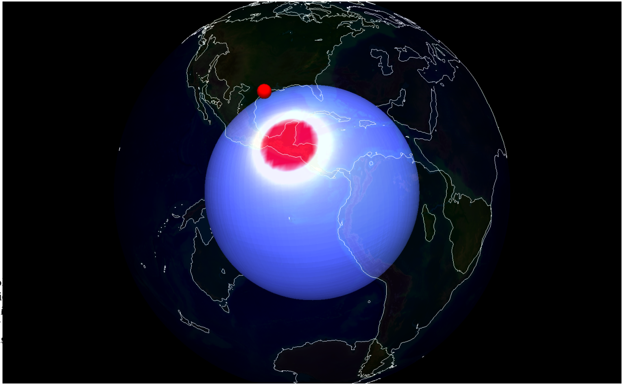

Gubbins and Roberts (1983)

The lithosphere is magnetized

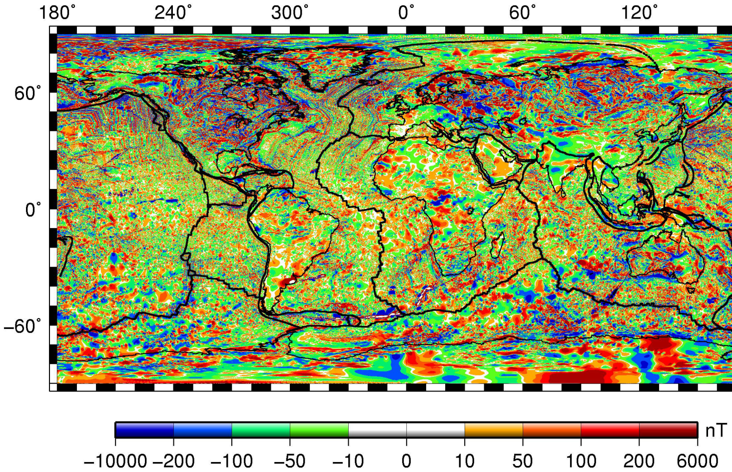

World Digital Magnetic Anomaly Map consortium

The geomagnetic field: a sparse record (in space and time)

A short-sighted view

- dipole-dominated
- small scales of dynamo field concealed by the small scales of the crustal field
- even if perfect sampling: $\ell \lesssim 13$ (lateral resolution of $\sim$ 1500 km at the core surface)

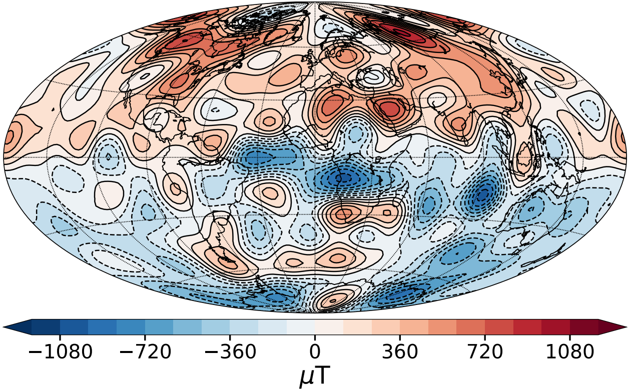

The geomagnetic field: a sparse record (in space and time)

A short-sighted view

- dipole-dominated
- small scales of dynamo field concealed by the small scales of the crustal field
- even if perfect sampling: $\ell \lesssim 13$ (lateral resolution of $\sim$ 1500 km at the core surface)

Time variations : constraints provided by geomagnetism (observatory ang satellite data)

- Smooth decadal variations punctuated by rapid (interannual) impulses (geomagnetic jerks)

Constraints provided by paleomagnetism

- The strength of the field varies on secular, millenial and geological time scales
- The further in the past we look, the cruder our description of the field (axial dipole)
- The field reverses its polarity every once in a while ($\approx$ 4 Myr^{-1} over the past 25 Myr)
- Last one 780 ka, poorly constrained transitional field

First-principle simulations can complement observations

Spherical harmonics: Pros and cons

Pros

- No pole problem
- Spectral convergence
- No need to solve for the exterior magnetic problem (Robin condition on the $\mathcal{P}^{B}_{\ell m}$)

$$\frac{\mathrm{d}\mathcal{P}^{B}_{\ell m}}{\mathrm{d}r} = -\frac{\ell}{r}\mathcal{P}^{B}_{\ell m} \text{ at } r = r_{\mathrm{CMB}}$$

Cons

- No operational fast Legendre transform: $O(\ell^2_{\mathrm{max}})$ cost
- Global basis: parallelization is not straightforward

The SHTns library

Schaeffer (2013)

- **Matrix-free algorithm**: computing recurrence on-the-fly is faster than reading from memory [unless maybe matrix-matrix product is used], and you save a lot of memory too.
- **Hand vectorized**, yet easily portable (currently supports Intel SSE2, AVX, AVX2+FMA, AVX512, CUDA).
- SHTns performance scales with microarchitecture: x2 for SSE2, x4 for AVX, x8 for AVX2+FMA, x16 for AVX512 (for large enough transforms).
  It also means the gap between classic implementations and SHTns will increase.
- Efficient **OpenMP parallelization**.
- Reaches 80% to 90% of peak performance on Intel SandyBridge.
- Accurate up to spherical harmonic degree $\ell = 16383$ (at least).
- **Free software**: https://bitbucket.org/nschaeff/shtns

What current geodynamo simulations can achieve

- ✓ produce a geomagnetic secular variation similar to the observed one
- ✓ generate a dipole-dominated field whose morphology at the CMB is similar to that of the recent geomagnetic field up to degree 13

Christensen et al. (2010): The Earth-likeness is controlled by 2 ratios of 3 time scales

$$E_\lambda = \frac{\tau_\Omega}{\tau_\lambda}$$

$$\mathrm{Rm} = \frac{\tau_\lambda}{\tau_{\mathrm{adv}}}$$

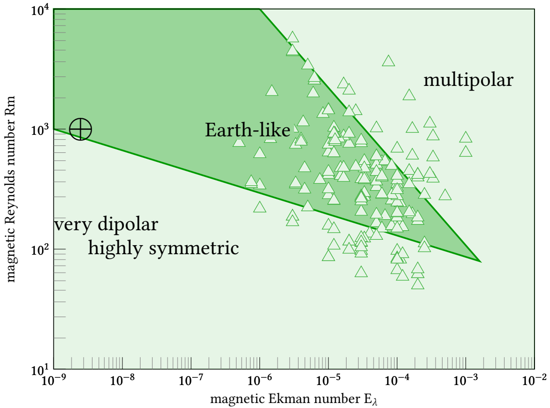

data courtesy U. Christensen